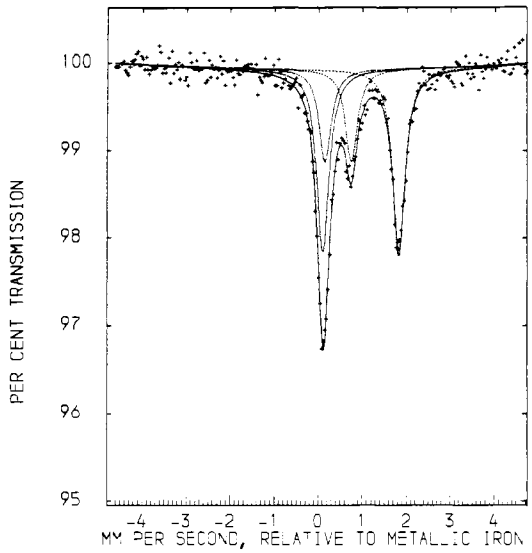

Figure 3. The 78 K Mössbauer-effect spectrum of a biphasic mixture containing the two limiting solid solutions. The major component is high-spin $Mn_{0.94}Fe_{0.06}S_2$. The minor component is low-spin $Mn_{0.04}Fe_{0.96}S_2$.

of the low-spin iron in $Mn_{0.04}Fe_{0.96}S_2$ prepared directly. The spectrum of this material shows no indication of the presence of an iron-containing sulfate impurity. The Mössbauer parameters for the iron site in $Mn_{0.94}Fe_{0.06}S_2$ indicate that in the MnS_2 lattice the iron adopts the high-spin, $^5T_{2g}$, electronic configuration. Our results are similar to those of Bargeron et al.,[8] who found that iron-57 as a dilute substitutional impurity in MnS_2 was high spin at pressures below ca. 40 kbar. Above this pressure, the iron is slowly converted with increasing pressure to the low-spin state.[8] In agreement with these authors,[8] we believe that the change in the electronic spin state of iron in going from FeS_2 to $Mn_{0.94}Fe_{0.06}S_2$ results from the reduction in the ligand field potential as the lattice parameter increases. The lattice parameter, a, for FeS_2 is 5.504 Å[8] whereas for MnS_2 it is 6.102 Å.[20] The proportions of the two iron-containing phases determined from the Mössbauer spectrum are in agreement with the starting composition and the observed phase limits, when the kinetic formation of pure MnS_2 is taken into consideration.

Our result for the solubility of MnS_2 in FeS_2 does not agree with the value of 5.6 mol % reported by Adachi et al.[9] Furthermore, our confirmation that $Mn_{0.04}Fe_{0.96}S_2$ contains low-spin iron(II) suggests that FeS_2 will be unable to accommodate the much larger high-spin manganese(II) ion and that the manganese(II) is present in the low-spin configuration. We have been unable to reproduce the preparation by using the method of Adachi et al.[9], and it is possible that they synthesized FeS_2 plus small quantities of (Mn,Fe)S. This interpretation would also account for their observation that the lattice parameter of their FeS_2 solid solution does not vary with manganese content. The greater solubility observed for iron in MnS_2 than for manganese in FeS_2 is consistent with the relative ease with which divalent iron can adopt either the high-spin or the low-spin electronic configuration.

Acknowledgment. It is a pleasure to acknowledge the assistance and the helpful discussions that we have had with Drs. G. Longworth and T. E. Cranshaw and Mr. B. Laundy during the course of this work. We also wish to thank the Science Research Council for a grant (GR/A/3320) toward the purchase of the electron microscope.

Registry No. FeS_2, 12068-85-8; MnS_2, 12125-23-4.

(20) Westrum, E. F.; Gronvold, F. *J. Chem. Phys.* **1970**, *52*, 3820.

Contribution from the Fachbereich Chemie und Sonderforschungsbereich 127 "Kristallstruktur und chemische Bindung" der Philipps-Universität Marburg, 3550 Marburg, GFR

Local and Cooperative Jahn-Teller Interactions of Copper(2+) in Host Lattices with Tetragonally Compressed Octahedra. Spectroscopic and Structural Investigation of the Mixed Crystals $K(Rb)_2Zn_{1-x}Cu_xF_4$

D. REINEN* and S. KRAUSE

Received September 29, 1980

The **g** tensor of the mixed crystals $K(Rb)_2Zn_{1-x}Cu_xF_4$ at high x values is exchange narrowed, corresponding to an antiferrodistortive order of elongated CuF_6 octahedra, with a distinct orthorhombic distortion component superimposed. At low x values the g parameters are in agreement with compressed octahedra in time average, with appreciable admixtures of $d_{x^2-y^2}$ into the d_{z^2} ground state, however. A model accounting for the change of g with x is proposed, which is based on the strain effect of the compressed ZnF_6 host lattice sites. The single-crystal and powder EPR data are supplemented by ligand field spectroscopic and structural information. In addition refined Cu-F bond lengths for K_2CuF_4 are given as the result of a neutron diffraction powder analysis. A set of approximate Jahn-Teller parameters (radial and angular distortion parameters ρ and φ, linear and nonlinear vibronic coupling constants V and V_3) for the mixed crystals with different Cu^{2+} concentrations could be evaluated, which is consistent with the available experimental information also for other copper(2+) fluoride compounds.

Introduction

Cu^{2+} ions in octahedral coordination undergo strong Jahn-Teller distortions, which correspond to a tetragonal elongation with frequently an orthorhombic symmetry component superimposed. This statement is correct only, however, if the host lattice sites are regularly octahedral and if the ligands are equal.[1] Cu^{2+} systems of this kind represent cases of strong linear Jahn-Teller coupling and the matrix[2]

$$\begin{pmatrix} {}^1/_2M\omega^2\rho^2 - V\rho\cos\varphi - V_3\rho^3\cos 3\varphi & V\rho\sin\varphi \\ V\rho\sin\varphi & {}^1/_2M\omega^2\rho^2 + V\rho\cos\varphi - V_3\rho^3\cos 3\varphi \end{pmatrix}$$

describes the energy changes occurring, if the electronic ^2E_g

0020-1669/81/1320-2750$01.25/0

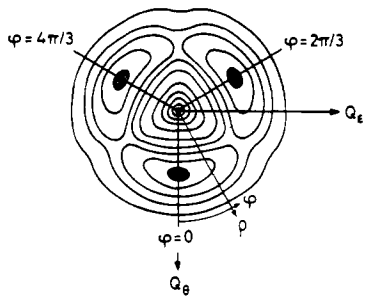

Figure 1. Cross section of lower potential surface–vibronic $E \times \epsilon$ interaction, linear and nonlinear coupling ($Q_\theta = \rho \cos \varphi$, $Q_\epsilon = \rho \sin \varphi$).

ground state undergoes vibronic interactions (V, $V_3 > 0$) with an octahedral vibration of the same symmetry (ϵ). In this matrix the various nonlinear coupling terms are represented by the third-order constant V_3. This simplified procedure has no influence on the symmetry of the problem and the essential conclusions derived. The resulting equation describes the well-known lower potential surface of the "Mexican hat", modified by a warping as the consequence of the nonlinear coupling. A cross section perpendicular to the E axis is shown in Figure 1, which also defines the radial and angular parameters ρ and φ. Minimizing with respect to ρ yields eq 1.

$$E_{\rho_0} = -E_{JT} - \beta \cos 3\varphi \qquad (1)$$

$$\left(E_{JT} = \frac{V_2}{2M\omega^2} = \tfrac{1}{2} V \rho_0; \quad \beta = V_3 \rho_0^3 \right)$$

The subsequent differentiation with respect to φ leads to minima at 0, 120, and 240°, which correspond to tetragonal elongations along the molecular z, x, and y axes of the octahedron. They are separated by saddlepoints at 180, 300, and 60°, which are correlated with tetragonal compressions along z, x, and y. The relations in eq 2 hold. In eq 2 the average

$$\rho_0 = (\sum_i 2\Delta i^2)^{1/2} \quad (a_i = \bar{a} + \Delta i, \text{ for } i = x, y, \text{ and } z)$$

$$\Delta i = \frac{\rho}{3^{1/2}} \cos (\varphi + \delta) \qquad (2)$$

(δ = 0, 240, and 120° for i = z, x, and y)

Cu^{2+}–ligand bond lengths are defined by $\bar{a} = {}^1/_3 \sum_i a_i$, which is true at least for smaller ρ values, where the center of gravity rule should be strictly valid.

If the host lattice site deviates in symmetry from O_h, the lower potential surface is deformed and the relative minima are shifted from their octahedral positions, stabilizing in general orthorhombic (or lower symmetry) Jahn–Teller deformations of the Cu^{2+} octahedron. It was of particular interest for us to stabilize the Jahn–Teller ion Cu^{2+} in a compressed instead of an elongated configuration. As we could demonstrate with the mixed crystals $Ba_2Zn_{1-x}Cu_xF_6$ at lower Cu^{2+} concentrations, this is indeed possible and obviously induced by the distinct axial compression of the ZnF_6 octahedra in this structure type.[3] A similar geometric property, but by far smaller in magnitude, is to be expected for K_2NiF_4-type lattices (Figure 2). A second important feature is the presence of elastic and electronic interactions between the CuF_6 polyhedra within the host matrix, which become effective with increasing Cu^{2+} concentration and lead to cooperative properties at high x values. The competing interplay

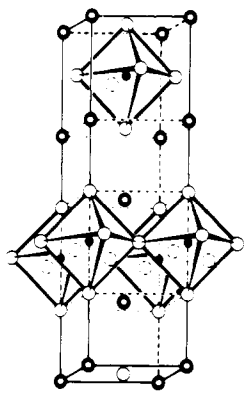

Figure 2. K_2NiF_4 structure.

between cooperative effects and the "host lattice strain" will lastly be deciding for the local deformations of the Cu^{2+} octahedra and their dynamic or static nature. We have followed the local distortion of the CuF_6 octahedra in dependence on x in the mixed crystals $K(Rb)_2Zn_{1-x}Cu_xF_4$ as model compounds mainly by single-crystal and powder EPR spectroscopy, supported by structural measurements and ligand field data, and could account for the appreciable shifts of the angular parameter by a simple model. The results of a powder neutron diffraction analysis of K_2CuF_4 on the basis of recent X-ray structure determinations[4] are presented in addition.

Experimental Section

Preparation. Very pure $A^I_2Zn_{1-x}Cu_xF_4$ compounds were obtained by fluorination (1 h at 150 °C, 3–5 h at 350 °C) of partly dehydrated Tutton salts $A^I_2Zn_{1-x}Cu_x(SO_4)_2 \cdot 6H_2O$ after a procedure described by Hoppe et al.[5] The yellow or yellow-brown products contained partly Cu^{3+}, as is obvious from the ligand field spectra, and were decomposed and sintered in vacuo (15 h at 150 °C, 40 h at 400 °C). The resulting mixed-crystal powders were white and quite sensitive to moisture. Single crystals were grown by heating the powder in sealed platinum tubes to 700–750 °C and subsequent cooling to room temperature within 3–5 days. The colorless crystals had the shape of thin plates with the tetragonal c axis perpendicular to the plate planes. The crystals were coated with colophonium before the physical measurements. The molar Cu^{2+}/Zn^{2+} ratio was determined by atomic absorption spectrometry and/or complexometric titration. The fluorine analyses performed were always consistent with the theoretical values within mostly less than 2% (relative). The mixed crystals $K_2Zn_{1-x}Ni_xF_4$ were synthesized by sintering stoichiometric mixtures of ZnF_2, NiF_2, and KHF_2 under vacuum (40 h at 550 °C).

Structural Measurements. The unit cell parameters were taken from X-ray powder diagrams [X-ray diffractometer (Philipps) Cu Kα radiation] with use of Au for calibration. The neutron diffraction measurements (298 K) on K_2CuF_4 were performed at the FR2 reactor of the Gesellschaft für Kernforschung in Karlsruhe. After one diagram was taken in the full range between $5.0° \leq 2\theta \leq 84.4°$ in steps of 0.1°, the 19 most intense reflection groups were measured again separately in steps of 0.05°. The analysis of the experimental data was based on the PERNOD program.[6]

Optical Measurements. The ligand field remission spectra were recorded by a Zeiss PMQ II spectrophotometer (Infrasil) with a low-temperature attachment. We used Sr_2ZnTeO_6 (4000–12000 cm^{-1}) and freshly sintered MgO (8000–30000 cm^{-1}) as standards.

EPR Measurements. The EPR spectra were taken with a Q-band E 15-Varian spectrometer and DPPH as internal standard ($g = 2.003_7$). A variable-temperature accessory (150–450 K) and low-temperature equipment (4.2 K) were available.

Results and Discussion

Structural Investigations. K_2ZnF_4 (a_0 = 405.6 pm, c_0 = 1311 pm, c_0/a_0 = 3.23) crystallizes in the K_2NiF_4 type (Z =

(1) D. Reinen and C. Friebel, *Struct. Bonding (Berlin)*, **37**, 1 (1979).
(2) See, for example: A. Abragam and B. Bleaney, "Electronic Paramagnetic Resonance of Transition Ions", Clarendon Press, Oxford, England, 1970, p 790 ff.
(3) C. Friebel, V. Propach, and D. Reinen, *Z. Naturforsch. B: Anorg. Chem., Org. Chem.*, **31B**, 1574 (1976).
(4) (a) R. Haegele and D. Babel, *Z. Anorg. Allg. Chem.*, **409**, 11 (1974); (b) E. Herdtweck and D. Babel, to be published.
(5) A. D. Westland, R. Hoppe, and S. S. I. Kaseno, *Z. Anorg. Allg. Chem.*, **338**, 319 (1965).
(6) S. Klein and H. Weitzel, *J. Appl. Crystallogr.*, **8**, 54 (1975).

Table I. Atomic Positions and Isotropic Temperature Parameters B for K_2CuF_4[a]

atom	position	point symmetry		z or x	B, Å^2
Cu(1)	4a	222	0, 0, 1/4; 0, 0, 3/4		0.68
Cu(2)	4d	222	0, 1/2, 0; 0, 1/2, 1/2		0.64
K(1), F(1)	8f	2	0, 0, z; 0, 0, $\bar{z}$; 0, 0, 1/2 + z; 0, 0, 1/2 − z	0.0730 (3),[b] 0.1733 (2)[c]	1.63[b] 1.11[c]
K(2), F(2)	8g	2	0, 1/2, z; 0, 1/2, $\bar{z}$; 0, 1/2, 1/2 + z; 0, 1/2, 1/2 − z	0.1818 (3),[d] 0.0767 (2)[e]	1.71[d] 1.30[e]
F(3)	8e	2	x, x, 1/3; $\bar{x}$, $\bar{x}$, 1/4; x, $\bar{x}$, 3/4; $\bar{x}$, x, 3/4	0.2252 (8)	0.64
F(4)	8h	2	x, 1/2 + x, 0; $\bar{x}$, 1/2 − x, 0; x, 1/2 − x, 1/2; $\bar{x}$, 1/2 + x, 1/2	0.2248 (8)	0.76

[a] Experimental data from neutron diffraction powder experiments. [b] K(1) value. [c] F(1) value. [d] K(2) value. [e] F(2) value.

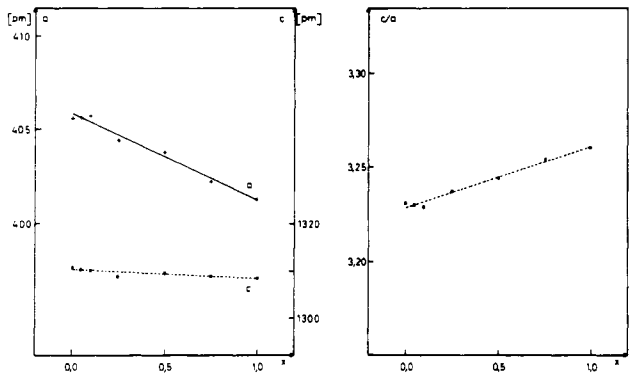

Figure 3. Unit cell parameters of mixed crystals $K_2Zn_{1-x}Ni_xF_4$ (a, $c \equiv a_0$, c_0).

2) of space group $I4/mmm$[7] (Figure 2). The lattice consists of nets of ZnF_6 octahedra, which are linearly connected with each other via common corners. There is a small anisotropy induced by the layer structure in the Zn–F bond lengths with two shorter spacings parallel to the tetragonal c axis and four longer ones in the (001) planes. The structural results with respect to the magnitude of this effect are somewhat contradictory. An older study[8] yields 3 pm for the difference in bond length between the four equatorial and the two axial ligands, while it is found to be less than 1 pm in a recent X ray single-crystal analysis[9] (Table III). The unit cell parameters of mixed crystals with K_2NiF_4 (a_0 = 401.$_3$ pm, c_0 = 1308 pm, c_0/a_0 = 3.26) exhibit ideal Vegard behavior (Figure 3).

K_2CuF_4 has a distorted K_2NiF_4-type structure, which is the result of a strong static Jahn-Teller deformation of the CuF_6 octahedra. The cooperative order of the polyhedra, which have orthorhombic symmetry but with the dominant component corresponding to a tetragonal elongation, is antiferrodistortive. This pattern was suggested from magnetic data[10] and EPR spectroscopy[11] already some years ago and lately confirmed by X-ray analysis.[4] The space group is $I4c2$ (Z = 8),[12] and the unit cell parameters are related to those of the K_2NiF_4 type by $a = 2^{1/2}\,a_0$ and $c = 2c_0$ (Figure 4). The atomic positions and Cu–F bond lengths found by Babel and co-workers[4] are given in Table II for comparison. The atomic layers perpendicular to [001] are visualized in Figure 5. Complete order ($c = 2c_0$) along [001] implies the layer sequence 1,2,3,4,3,2,5,2,3,6,3,2,1. A disorder along this direction (c = c_0), which is most frequently found,[4] corresponds to a sequence 1(5),2,3,4(6),3,2,1(5).

The groups of reflections, which mainly determine the F^- positions (hkl with h, $k = 2n$, $l = 4n + 2$ and h, $k \neq 2n$, $l = 4n$ as well as those with $l \neq 2n$) are very weak, however.

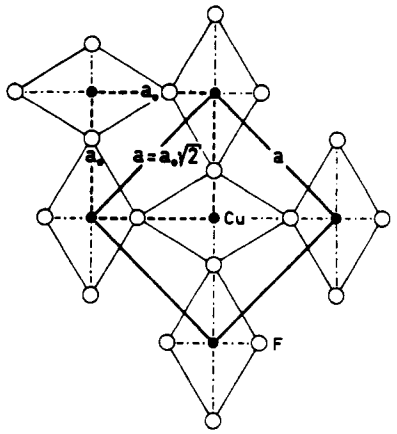

Figure 4. Antiferrodistortive order of CuF_6 polyhedra in the (001) planes of K_2CuF_4.

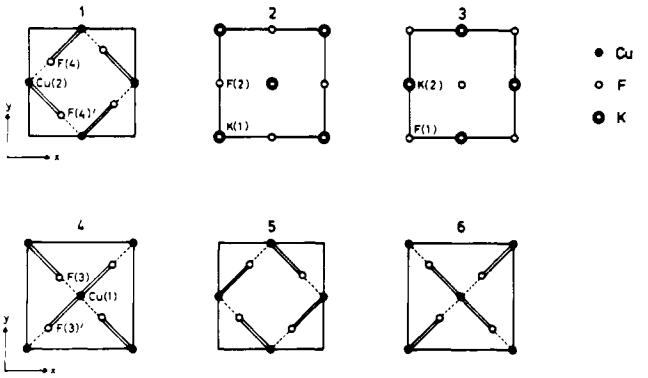

Figure 5. Sequence of planes along [001] in K_2CuF_4 (see text) (═ and --- represent long and short Cu–F bond lengths, respectively).

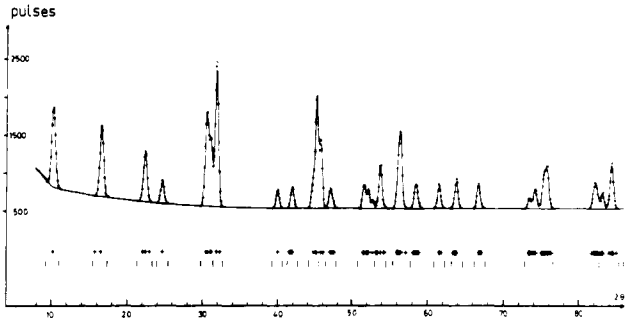

Figure 6. Neutron diffraction powder diagram of K_2CuF_4 (separately measured reflection groups).

(7) D. Balz and K. Plieth, *Z. Elektrochem.*, **59**, 545 (1955).
(8) O. Schmitz-DuMont and H. Bornefeld, *Z. Anorg. Allg. Chem.*, **287**, 120 (1956).
(9) E. Herdtweck and D. Babel, *Z. Kristallogr.*, in press.
(10) D. J. Khomskii and K. J. Kugel, *Solid State Commun.*, **13**, 763 (1973).
(11) C. Friebel and D. Reinen, *Z. Anorg. Allg. Chem.*, **407**, 193 (1974).
(12) Recently, an orthorhombic space group (*Bbcm*) is claimed for K_2CuF_4: M. Hidako and P. J. Walker, *Solid State Commun.*, **31**, 383 (1979). This is not supported by our EPR results. The **g** tensor perpendicular to [001], which is exchange narrowed and hence reflects the symmetry of the (001) planes, neither shows a splitting in the powder spectra nor exhibits any angular dependence.

Table II. Interatomic Spacings (pm) in K_2CuF_4

		Neutron Diffraction Data			
Cu(1)-F(1)	194.9 (5)	K(1)-F(1)	254.9 (13)	F(1)-F(3)	269.7 (8)
Cu(1)-F(3)	186.4 (7)	K(1)-F(2)	292.9 (13)	F(1)-F(3)	299.6 (8)
Cu(1)-F(3)	227.5 (7)	K(1)-F(4)	263.0 (10)	F(2)-F(4)	269.5 (8)
Cu(2)-F(2)	194.9 (5)	K(2)-F(2)	267.1 (13)	F(2)-F(4)	299.8 (8)
Cu(2)-F(4)	186.1 (7)	K(2)-F(1)	293.5 (13)	F(3)-F(3)	294.1 (13)
Cu(2)-F(4)	227.8 (7)	K(2)-F(3)	254.5 (10)	F(4)-F(4)	294.2 (13)
Cu-F(av)	203 (1)	K-F(av)	274 (1)	F-F(av)	288 (1)
		Cu-F Spacings			
Cu-F(1,2)	192 (2)[a]		194.9 (5)[b]		193.9 (2)[c]
Cu-F(3,4)	192 (4), 222 (4)		186.3 (8), 227.6 (8)		190.9 (7), 223.8 (7)

[a] X-ray data from crystal with $c = 2c_0$.[4a] [b] This work. [c] X-ray data from crystal with $c = c_0$.[4b]

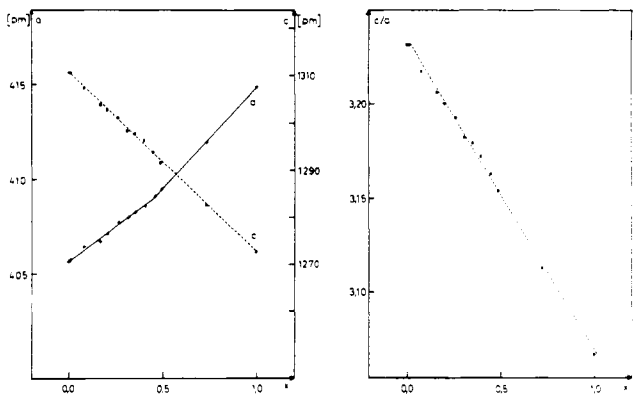

Figure 7. Unit cell parameters of mixed crystals $K_2Zn_{1-x}Cu_xF_4$ (a, $c \equiv a_0$, c_0].

In order to refine in particular the Cu–F bond lengths, we performed a neutron diffraction powder analysis on the basis of the X-ray structural data. The powder diagram and the derived atomic parameters and bond lengths for K_2CuF_4 (a = 585.4 pm, c = 2542 pm) are given in Figure 6 and Tables I and II. Twenty-three reflection groups were measured, the number of independent variables was 18, and the final reliability factors[6] obtained were

$$R_c = \frac{\sum_{hkl}(I_{hkl}^0 - SI_{hkl}^c)}{\sum_{hkl} I_{hkl}^0} = 0.028$$

$$R_p = \frac{\sum_{2\theta}(I_{2\theta}^0 - SI_{2\theta}^c)}{\sum_{2\theta} I_{2\theta}^0} = 0.039$$

The introduction of disorder along c leads to larger R values. From the neutron diffraction data a strong orthorhombic distortion component of the otherwise elongated CuF_6 octahedra is immediately evident. The intermediate bond length (195 pm) extends along the c axis, and the short and long Cu–F spacings (186.5 and 227.5 Å) are located in the (001) plane. With use of eq 2 a ρ_0 value of 43 pm is calculated, while the angular parameters, which characterize the two sublattices constituting the antiferrodistortive order, are φ_0 = 109 and 251°, respectively (Table III, Figure 4).

The unit cell parameters of the mixed crystals $K_2Zn_{1-x}Cu_xF_4$ demonstrate the specific influence of the Jahn–Teller unstable Cu^{2+} ion. The unit cell parameter c decreases, while a becomes larger with increasing x (Figure 7). The concentration dependence is completely different from the one for $K_2Zn_{1-x}Ni_xF_4$ (Figure 3), though the unit cell volumes of $K_2T^{II}F_4$ with T^{II}: Ni,Zn,Cu differ only slightly (211, 216, and 219 × 10^6 pm, respectively). Because it was not possible—even for K_2CuF_4—to see the weak superstructure reflections, mentioned above, in the X-ray powder diagrams, the smaller K_2NiF_4-type unit cell was taken as a basis for the indexing. The change in slope for a vs. x at $x \simeq 0.45$ possibly indicates the transition from space group $I4/mmm$ to $I4c2$. With acceptance of this suggestion, the larger increase of a above the critical concentration would then be induced by long-range cooperative ordering of the CuF_6 polyhedra. A variation in slope for c vs. x at the same concentration must not necessarily occur, because the Cu–F bond lengths parallel to [001] can be easily adjusted by a slight change of the z parameter of F(2) (Table I). Though less experimental data are available for the $Rb_2Zn_{1-x}Cu_xF_4$ mixed-crystal series, a distinct break in the linear dependence of a vs. x—but in this case for c and c/a as well— is also observed. The critical concentration for the inset of long-range cooperative ordering seems to be considerably lower ($x \approx 0.3$), however.

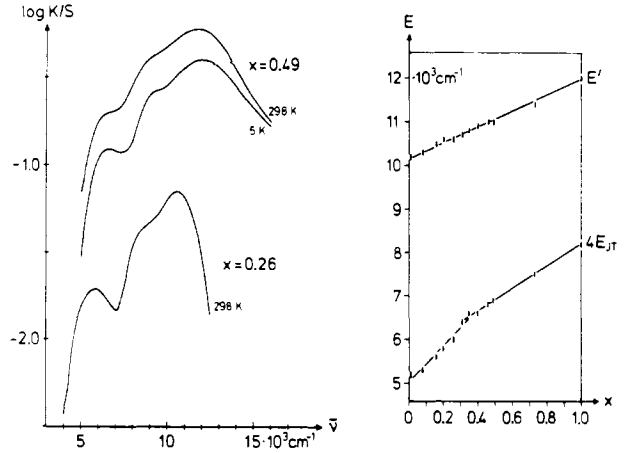

Figure 8. Dependence of the lowest ($4E_{JT}$) and highest energy transition (E') on x (right) and ligand field spectra for x = 0.26 and 0.49 (left) for $K_2Zn_{1-x}Cu_xF_4$ (compare Figure 9).

Ligand Field Spectroscopy. While the energies of the ligand field transitions are independent on x for mixed crystals $K_2Zn_{1-x}Ni_xF_4$ (Δ = 7400 cm^{-1}, B = 960 cm^{-1}, C/B = 4.2), a distinct shift of the three-band spectrum to higher energies with increasing Cu^{2+} concentration is observed for the corresponding Cu^{2+} compounds (Figure 8). The appearance of three bands clearly indicates the presence of tetragonally distorted CuF_6 octahedra, with possibly an unresolved lower-symmetry component superimposed (Figure 6). Because it can be assumed that the octahedral ligand field parameter Δ_0 is independent on x—analogous to Ni^{2+} in the same K_2ZnF_4 host lattice—the observed spectral energy shifts have to be interpreted as caused by an increasing extent of the local Jahn–Teller distortions with increasing Cu^{2+} concentration.

(13) C. Billy and H. M. Haendler, *J. Am. Chem. Soc.*, **79**, 1049 (1957).
(14) A. Okazaki and Y. Suemune, *J. Phys. Soc. Jpn.*, **16**, 176 (1961).
(15) D. Reinen and H. Weitzel, *Z. Naturforsch. B: Anorg. Chem., Org. Chem.*, **32B**, 476 (1977).
(16) O. Schmitz-DuMont and D. Grimm, *Z. Anorg. Allg. Chem.*, **355**, 280 (1967).
(17) H. G. v. Schnering, *Z. Anorg. Allg. Chem.*, **353**, 14 (1967).
(18) D. W. Smith, *Struct. Bonding (Berlin)*, **12**, 49 (1972).

Table III. Structural, Ligand Field, and Jahn-Teller Energy Parameters for Copper(2+) Fluoride Compounds

	Cu-F,[b] pm	ligand field energies (10^3 cm^{-1}) [5 K] E(I)	E(II)	E(III)	Δ_0	K_σ,[c] 10^6 cm^{-1}	ρ_0, pm	V, cm^{-1} pm^{-1}	φ_0,[d] deg
CuF_2	193 (4x)[13] 227 (2x)	7.5	8.8	11.4	6.8[16]	0.82	39	96	0
$KCuF_3$[a]	196 (2x)[14] 189 (2x) 225 (2x)	7.8	9.1	11.8	7.0	0.83	38	102.$_5$	109, 251 106, 254
Ba_2CuF_6[a]	185 (2x)[15] 193.$_5$ (2x) 232.$_5$ (2x)	9.8	10.0	(12.0) 13.3	6.9[3]	0.82	50.$_5$	97	130, 230 134, 226
K_2CuF_4[a]	192 (2x)[4a] 192 (2x) 222 (2x)	8.2	9.3	12.0	7.0[11]	0.95	35	117	120, 240
	195 (2x) 186.$_5$ (2x) 227.$_5$ (2x)					0.79	43	95.$_5$	109, 251 105, 255
	194 (2x)[4b] 191 (2x) 224 (2x)					0.92	36.$_5$	112.$_5$	115, 245 114, 246

[a] Zn-F bond lengths (pm) in host lattices are as follows: $KZnF_3$ 203 (6x); Ba_2ZnF_6 196 (2x), 205 (4x)[17] (ρ_0 = 10.$_5$); K_2ZnF_4 198 (2x) 201 (4x)[8] (ρ_0 = 3.$_5$), 202.$_5$ (2x), 203 (4x)[9] (ρ_0 = 0.$_5$). [b] In the case of antiferrodistortive order, the bond lengths parallel to [001] are underlined. [c] The used S_σ overlap integrals are those tabulated by Smith.[18] [d] Calculated from eq 2 and 4: first and second lines, respectively. The two values refer to the sublattices constituting the antiferrodistortive order.

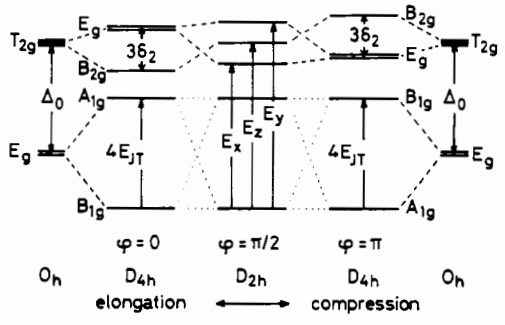

Figure 9. Energy level diagram of Cu^{2+} in octahedral coordination and in the presence of tetragonal and orthorhombic distortions [$\Delta_0 \equiv {}^1/_3(E_x + E_y + E_z) - 2E_{JT}$ (assuming the validity of the center of gravity rule)].

This view is strongly supported by the dependence of the ground-state splitting (lowest energy band) on x, which is approximately twice as large as the shift of the highest energy band with the Cu^{2+} concentration (Figures 8 and 9). $4E_{JT}$ changes from 5200 cm^{-1} for x = 0.01 to 8200 cm^{-1} for K_2CuF_4. Band shifts of comparable magnitudes in the spectra of Cu^{2+} in octahedral coordination have been reported for various fluoridic and oxidic mixed-crystal systems, which could be interpreted consistently in an analogous way.[1] The relative band intensities correspond to those, which are usually observed for elongated octahedra. Because the half-widths of the bands is appreciable, an additional but masked splitting of the higher energy double band (orthorhombic component, Figure 9) may be also present. This subject will be taken up below again. Mixed crystals $Rb_2Zn_{1-x}Cu_xF_4$ exhibit analogous characteristics.

The splitting of the ^2E_g octahedral ground state is directly related to the extent of the radial distortion of the CuF_6 octahedra. This is immediately seen, if a description in terms of the "angular overlap model"[19] (AOM) is chosen. For D_{2h} symmetry one obtains eq 3, where $e_\sigma^i = K_\sigma S_\sigma^i$ with $i, j = x$,

$$E_{JT} = \frac{1}{2}\rho_0 V = \frac{1}{2}\left[\sum_i e_\sigma^{i2} - \frac{1}{2}\sum_{ij}^{i\neq j} e_\sigma^i e_\sigma^j\right]^{1/2} \qquad (3)$$

y, z. The energy parameters e_σ^i are proportional to the squares of the standard overlap integrals S_σ^i along the molecular x, y, and z axes. The angular distortion is equally related to the AOM energy parameters (eq 4).

$$\varphi_0 = \arctan 3^{1/2}\frac{e_\sigma^x - e_\sigma^y}{2e_\sigma^z - (e_\sigma^x + e_\sigma^y)} \qquad (4)$$

In Table III distortion parameters ρ_0 and φ_0, AOM parameters K_σ, and linear Jahn-Teller coupling constants V are collected for some copper(2+) fluoride compounds. They have been calculated from available structural and ligand field data, with use of Equations 2–4. The radial vibronic energy for the compounds of Table III are calculated from eq 5 to be $\hbar\omega$ =

$$\rho_0 = \frac{V}{M\omega^2} \qquad (5)$$

200 ± 15 cm^{-1}. The angular parameters derived from the AOM energies deviate more strongly from φ = 120 and 240° than those obtained from eq 2. The reason is possibly the nonvalidity of the center of gravity rule, which is not presumed for eq 4. The refined Cu–F bond lengths for K_2CuF_4 are more consistent with the comparable data of related compounds than both X-ray results and should hence be a reliable basis for the interpretation of the EPR parameters discussed below. The distortion of the CuF_6 polyhedra in K_2CuF_4 is larger in magnitude than the one in $KCuF_3$, which crystallizes in a tetragonally deformed perovskite structure. The orthorhombic symmetry component is about the same in both compounds, however, with the Cu–F bonds of intermediate length orientated parallel to [001]. In Ba_2CuF_6, in which the polyhedra are even more strongly distorted, the shortest Cu–F bond length is found to be the one in the [001] direction. The reason is most probably the appreciable host lattice effect, i.e., the ZnF_6 octahedra, which are considerably compressed in the axial directions parallel to [001] (ρ_0 = 10.5 pm, Table III). This strain obviously shifts the sublattice distortions toward φ values larger than 120° and smaller than 240°. Though K_2CuF_4 is imposed to a host lattice strain of the same symmetry, the ZnF_6 site compression in K_2ZnF_4 is by far smaller. Though we are aware of the rather approximate magnitude of this value, we will choose $\rho_0 \simeq 3$ pm (Table III) to describe the strain effect in K_2ZnF_4 in the discussion below.

An estimate of the radial distortion of the CuF_6 polyhedra in mixed crystals with $x < 1$ is also possible, if the coupling

(19) C. K. Jørgensen, *Struct. Bonding (Berlin)*, **1**, 3 (1966).

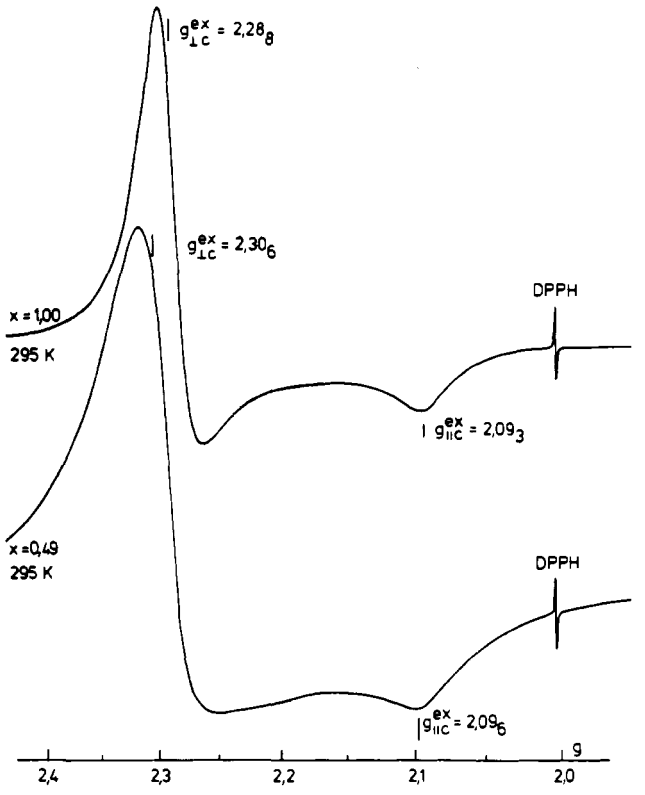

Figure 10. EPR powder spectra of mixed crystals $K_2Zn_{1-x}Cu_xF_4$ with $x > 0.45$.

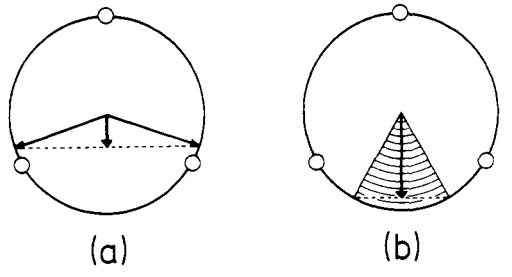

Figure 11. Angular distortions of mixed crystals $K_2Zn_{1-x}Cu_xF_4$: (a) angular parameters of the sublattices, which constitute the antiferrodistortive order in K_2CuF_4, and resulting unit cell deformation; (b) dynamical averaging and resulting distortion for $x \approx 0.1$. Circles represent positions of tetragonal elongation at 0, 120, and 240°.

constant V is considered to be the same as for K_2CuF_4. With use of the experimental E_{JT} energies (Figure 8) the following ρ values are obtained:

x	0.01	0.08	0.26	0.46	0.73	(A)
ρ_0, pm	$27._5$	28	$31._5$	$35._5$	$39._5$	

EPR Spectroscopy. In the range of *Cu^{2+} concentrations 1.0* $\gtrsim x \gtrsim 0.4_5$ a tetragonal **g** tensor with $g(\perp c) > g(\parallel c) > g_0$ ($g_0 = 2.00_2$) is found between 298 and 77 K (Figure 10). The single-crystal EPR spectra show only one signal, and no angular dependence of $g(\perp c)$ in the (001) plane is observed. As was demonstrated in a recent paper,[11] the **g** tensor is exchange narrowed according to the antiferrodistortive order of essentially elongated CuF_6 octahedra (Figure 4). The g values for one of the orthorhombic sublattices (Figure 11a) are given in eq 6 ($g_0 = 2.002_3$, $u_i = k_i^2\lambda_0/E_i$ ($i = x, y, z$) with $E_{x[y,z]}$ defined in Figure 9, $\lambda_0 = 830$ cm^{-1}).

$$g_x = g_0 + 4u_x[1 + \cos(120° - \varphi_0)]$$
$$g_y = g_0 + 4u_y[1 + \cos(120° + \varphi_0)] \quad (6)$$
$$g_z = g_0 + 4u_z[1 + \cos\varphi_0]$$

Table IV. g Values for Mixed Crystals $K(Rb)_2Zn_{1-x}Cu_xF_4$ with $x \gtrsim 0.25$

x		T, K	$g^{ex}(\parallel c)$	$g^{ex}(\perp c)$
		Potassium Compounds		
1.0	p, s[a]	298	2.09_3	2.28_5
		77	2.08_7	2.27_9
0.7_3	p	298, 100	2.09_6	2.29_9
0.4_8, 0.4_6	p	298, 100	2.09_5	2.30_5
0.26	s	450	2.07_5	2.32_9
		350	2.06_8	2.33_2
		250	2.05_6	2.33_3
		150	2.04_5	2.33_3
		Rubidium Compounds		
1.0	p	295, 100	2.08_8	2.28_1
0.5	p	295, 100	2.09_0	2.29_5

[a] s = single-crystal data and p = powder data.

Exchange narrowing in the plane containing the molecular x (long) and y (short) axes yields the cooperative g parameters[12] in eq 7. With the simplifications $u_x = u_y = u_\perp$, $u_z = u_\parallel$, and $k_\parallel = k_\perp = k$ we were able to estimate the magnitudes of the angular parameter φ, the covalency factor k, and the molecular g values from the experimental data of Table IV and Figure 8, with use of eq 6 and 7, which were extended by the inclusion of third-order orbital contributions, however. The calculated parameters are given in eq 8.

$$g^{ex}(\parallel c) = g_z \qquad g^{ex}(\perp c) = \frac{1}{2}(g_x + g_y) \quad (7)$$

$$\varphi_0 \simeq 118\ (1)° \qquad k \simeq 0.84\ (1) \qquad g_x \simeq 2.50\ (1)$$
$$g_y \simeq 2.08\ (1) \qquad g_z \simeq 2.09_{5\,(5)} \quad (8)$$

Surprisingly a much smaller orthorhombic distortion component is obtained than the one derived from neutron diffraction. An anisotropy in the covalency factor with $k_\perp < k_\parallel$ will move the sublattices toward the experimental φ values, however. A noticeable change of φ with decreasing x is not observed though ρ changes considerably.

The 4.2 K EPR powder spectra of the mixed crystals in the concentration range discussed so far indicate the presence of long-range magnetic ordering (Figure 12). The **g** tensor is still tetragonal, but the g values have shifted due to the presence of internal fields. The average internal field can be estimated from eq 9 to be $H_\parallel{}^i \approx 2200$ Oe and $H_\perp{}^i \approx -1000$ Oe. H, g

$$\frac{H_{\parallel(\perp)}{}^i}{H_{\parallel(\perp)}} = \frac{g_{\parallel(\perp)}}{g_{\parallel(\perp)}'} - 1 \quad (9)$$

and H' ($\equiv H + H^i$), g' refer to the high- and low-temperature spectra, respectively. A similar striking temperature change in the EPR spectrum is reported for Ba_2CuF_6[3] as well, indicating ferromagnetic ordering at low temperatures in this compound also. The single-crystal EPR spectra of K_2CuF_4 at 4.2 K seem to give evidence of magnetic domains of varying sizes and with different orientations to the external magnetic field. The signals of these domains overlap and extend over a Δg range of 0.3–0.4 for each orientation (Figure 12). The angular dependence of the **g** tensor in the planes containing the crystallographic [001] direction has the same shape as the one at high temperatures, however. The transition from one spectrum to the other is reversible and takes place already at about 30 K, far above the Curie temperature ($T_c = 6.2_5$ K[20]).

EPR single-crystal spectra of mixed crystals in the *concentration range* $0 < x \lesssim 0.1$ exhibit only one signal, and the **g** tensor is tetragonal with $g(\perp c) > g(\parallel c) > g_0$, as observed

(20) N. Hirakawa and H. Ikeda, *J. Phys. Soc. Jpn.*, **35**, 1328 (1973).

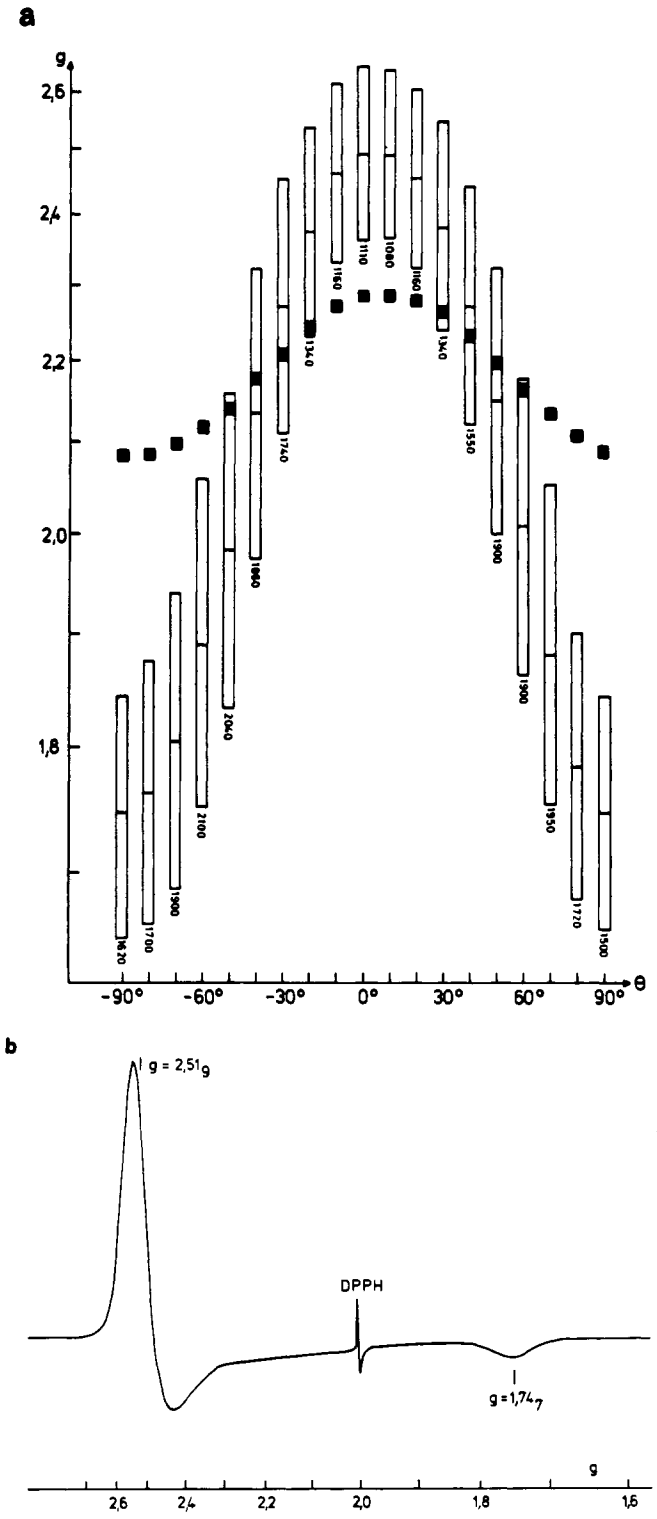

Figure 12. EPR spectra of K_2CuF_4: angular dependence of the **g** tensor, in a plane containing the unit cell *c* axis, for 298 (■) and 4.2 K (□) [*g* range of overlapping signals (numbers give the range in Oe)] (a); powder spectrum at 4.2 K (b).

for $x \gtrsim 0.4_5$ also. Again $g(\perp c)$ shows no angular dependence in the (001) plane. The $g(\|c)$ value is very near g_0 this time (Table V, Figure 13), however, suggesting Cu^{2+} in tetragonally compressed octahedra at the first sight. For this geometry the *g* values are expected to be

$$g_\| = g_0 - 3u^2 \qquad g_\perp = g_0 + 6u - 6u^2 \tag{10}$$

if anisotropies in the orbital contributions *u* are not accounted for. Equation 10 corresponds to $\varphi = 180°$ and a pure d_{z^2}

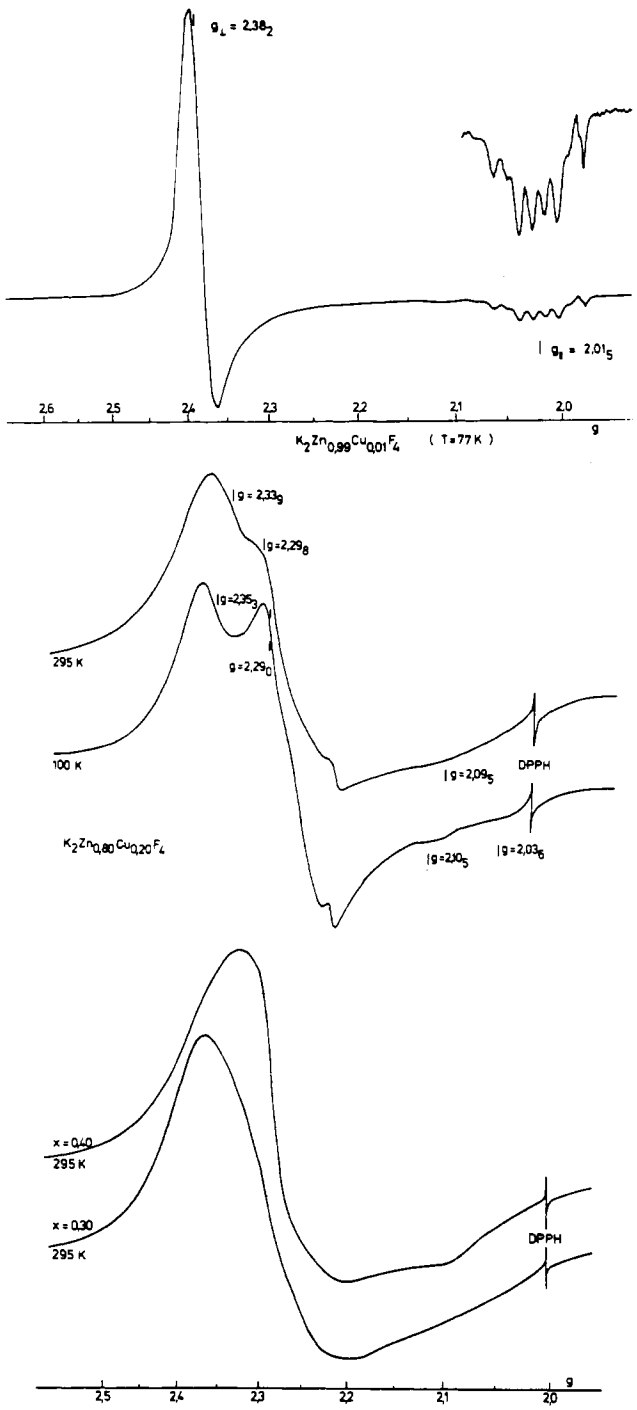

Figure 13. EPR powder spectra of mixed crystals $K_2Zn_{1-x}Cu_xF_4$ (x = 0.01, 0.20, 0.30, 0.40).

ground state. The slight, but distinct deviation of $g(\|c)$ from $g_0 - 3u^2$ indicates an admixture of $d_{x^2-y^2}$, however. If one defines $\varphi = 180° \pm 2\alpha$ with α describing the electronic delocalizaton, the ground-state wave function and the **g** tensor are given by eq 11.

$$\Phi_g = \cos\alpha(d_{z^2}) \mp \sin\alpha(d_{x^2-y^2})$$
$$g_\| = g_0 + 8(\sin^2\alpha)u - (3 + 4\sin^2\alpha)u^2 \tag{11}$$
$$g_\perp = g_0 + 2(3 - 2\sin^2\alpha)u - 2(3 - \sin^2\alpha)u^2$$

The interpretation of the EPR data in Table V as molecular *g* values corresponding to eq 11 is further supported by the well-resolved hyperfine structure in $g(\|c)$ (Figure 13). Obviously the CuF_6 polyhedra lie fairly isolated from each other in the K_2ZnF_4 host matrix. From the experimental *g* param-

Table V. g Values and Delocalization Parameters 2α for Mixed Crystals $K(Rb)_2Zn_{1-x}Cu_xF_4$ with $x < 0.1$

x		T, K	$g_\parallel$	$g_\perp$	2α, deg
		Potassium Compounds			
0.01	p[a]	298	2.04_2	2.36_9	37
		77	2.01_5	2.38_2	26
		4.2	2.01_0	2.38_9	24
0.05	s	298	2.04_3	2.36_0	$37._5$
		170	2.01_6	2.36_9	$26._5$
	p	298	2.04_5	2.36_8	38
		100	2.02_3	2.37_8	29
0.08	p	298	2.04_5	2.37_1	38
		100	2.03_6	2.38_0	35
		77	2.02_8	2.39_2	$31._5$
		4.2	2.02_0	2.39_6	$28._5$
		Rubidium Compounds			
0.01	p	298	2.03_1	2.37_9	33
		100	2.01_3	2.38_4	25

[a] s = single crystal data and p = powder data.

eters and ligand field data we have calculated the 2α values listed in Table V. The orbital contributions were considered as isotropic ($u = k^2\lambda_0/E$), and the average energy of the higher wavenumber double band (Figure 8) was taken for E. With respect to the introduced simplifications the obtained k factors of 0.90 (1) are reasonable.

The simple model outlined below is proposed to explain semiquantitatively the experimental g parameters and their dependence on the Cu^{2+} concentration. It has already been successfully used to account for the EPR and ligand field data of $Ba_2Zn_{1-x}Cu_xF_6$ mixed crystals.[3] As was mentioned above, one may regard the deviation of the ZnF_6 host lattice site from O_h symmetry as a strain imposed on the lower potential surface in Figure 1. The strain energy has the same symmetry as the linear Jahn–Teller coupling, namely, the two components[21]

$$G_\theta^s = \gamma\rho_s \cos\delta_s \qquad G_\epsilon^s = \gamma\rho_s \sin\delta_s \quad (\gamma > 0) \tag{12}$$

Extending the aforementioned matrix by adding $\pm G_\theta^s$ to the diagonal and G_ϵ^s to the nondiagonal energies and considering the strain energy as small with respect to E_{JT} replace eq 1 by eq 13. Restricting to a strain with the symmetry of a tet-

$$E_{\rho_0} = -E_{JT} - \beta\cos 3\varphi - b\cos(\varphi - \delta_s) \quad (b = \gamma\rho_s) \tag{13}$$

ragonal compression ($\delta_s = 180°$) and minimizing eq 13 with respect to φ reveal the additional minima imposed on the ringlike $E_{\rho 0}$ positions, which are modified compared to Figure 1, however. The following φ_0 values result:

$$\begin{aligned} &b < 9\beta\text{: 3 minima at } \varphi_0 = 0° \text{ and arc cos}\left[-\frac{1}{2}\left(1+\frac{b}{3\beta}\right)^{1/2}\right] \text{ and} \\ &\text{3 saddlepoints at } \varphi_0 = 180° \text{ and arc cos}\left[+\frac{1}{2}\left(1+\frac{b}{3\beta}\right)^{1/2}\right] \\ &b \geq 9\beta\text{: 1 minimum at } \varphi_0 = 180° \text{ and 1 saddlepoint at } \varphi = 0° \end{aligned} \tag{B}$$

Potential curves for different b/β ratios [eq 13 and (B)] are shown in Figure 14. The delocalization angles 2α listed in Table V reflect the double-minimum structure symmetrical to the saddlepoint at 180°. In particular the 4.2 K values, which most probably originate from the lowest vibronic state, may be interpreted as the angular parameters of the two minimum positions in first approximation. On this basis the following φ_0 values and energies are calculated, which correspond to $2\alpha = 24$ and $28._5°$, respectively (compare Table V; $x = 0.01, 0.08$):

$$\begin{aligned} &x = 0.01 \rightarrow b/\beta = 7.0\text{: minima at } 156, 204\ (-6.1\beta), \text{ and } 0°\ (6.0\beta) \\ &\text{and saddlepoints at } 24, 336\ (6.1\beta), \text{ and } 180°\ (-6.0\beta) \\ &x = 0.08 \rightarrow b/\beta = 6.3\text{: minima at } 151._5, 208._5\ (-5.4_5\beta), \text{ and } 0° \\ &(5.3\beta) \text{ and saddlepoints at } 28._5, 331._5\ (5.4_5\beta), \text{ and } 180°\ (-5.3\beta) \end{aligned} \tag{C}$$

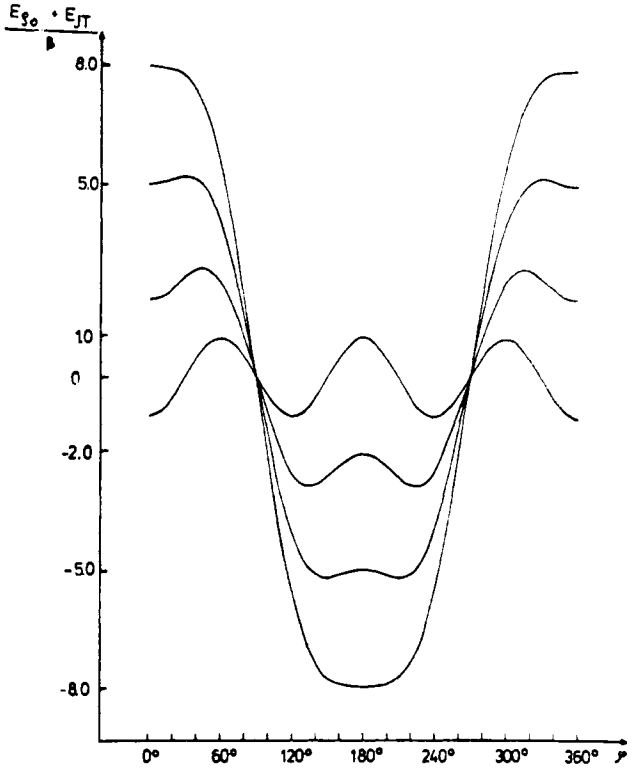

Figure 14. Warping of the lower potential curve of the Mexican hat (cross sections) due to the influence of nonlinear Jahn–Teller coupling and strain (eq 13 with $\delta_s = 180°$) [for $b/\beta = 9$, 6, 3, and 0 from below, with b and β defined in the matrix and eq 13; angular parameter φ displayed as a linear coordinate].

The energy barrier separating the two minima is less than 0.2β. If the lowest vibronic state in either of the two minima has an energy, which exceeds this value, an averaged **g** tensor with a delocalization behavior expressed by $\pm 2\alpha$ should be observed. We are aware, however, that the experimental 2α angles cannot be identified with the two minimum positions *exactly* in such a case, because they also contain contributions that are due to the zero-point vibration and lead to an additional mixing of $d_{x^2-y^2}$ into the ground state.[22] A thermal population of the third minimum at $\varphi = 0°$ can be excluded at least at lower temperatures, because an energy of more than 10β is afforded.

In order to get a more quantitative understanding, we may do some admittedly crude estimations and examine afterward if they are consistent with the physical reality. The strain imposed on Cu^{2+} by the host lattice is $b = \gamma\rho_s$ (eq 12), which yields $\simeq 300$ cm^{-1} [with $\rho_s \simeq 3$ pm and $\gamma \simeq V(K_2CuF_4)$]. With this strain energy the nonlinear coupling constant V_3 and the energy barriers Δ at $\varphi = 180°$ can be calculated for the mixed crystals with $x \lesssim 0.1$:

x	ρ_0, pm [(A)]	β, cm^{-1}	Δ, cm^{-1}	V_3, cm^{-1} pm^{-3}	V/V_3, pm^2
0.01	$27._5$	$\simeq 43$	≈ 4	$\simeq 2.2 \times 10^{-3}$	$\simeq 4.4 \times 10^4$
0.08	28	$\simeq 48$	≈ 7		

(D)

The very small Δ energies are indeed in agreement with a delocalization behavior involving the two minima symmetrically to $\varphi = 180°$. The minimum at 0° is more than 500 cm^{-1} higher in energy. It seems doubtful, that the unusually large temperature dependence of the g values (Table V) is caused by a population of this level. A more obvious reason for the

(21) R. Englman, "The Jahn-Teller effect in Molecules and Crystals", Wiley-Interscience, New York, 1972, pp 124–132 and 173–180.
(22) C. Friebel, W. Henke, M. Hitchman, and D. Reinen, in preparation.

temperature effect is the broad and high potential curve (Figure 14, $b/\beta = 6$), in which thermally more easily accessible excited vibronic levels may extend over a φ range of 180° and even more. The temperature dependence of the **g** tensor in this and other systems, which are subject to nonrandom strain, is discussed separately.[22] The bond lengths of the molecular x and y axes, located in the (001) planes of the lattice, fluctuate between the values which are given by the respective φ_0 parameters of the two minima and by ρ_0 ((D)) and are accessible from eq 2, if the average Cu–F spacing is 203 pm:

x	a_z, pm	$a_{x(y)}$, pm	$a_{y(x)}$, pm	
0.01	189	204*	216*	(E)
0.08		203*	217*	

The asterisked values are dynamically averaged to 210 pm in the (001) plane. The rather large radial and angular distortions already at low Cu^{2+} concentrations, which exceed the one expected from Figure 7, give evidence that the neighboring ZnF_6 octahedra are strongly taking part in matching the considerable local Cu^{2+} Jahn–Teller deformations to the less asymmetric host lattice.

Further arguments supporting our model come from the EPR spectra of mixed crystals $Ba_2Zn_{1-x}Cu_xF_6$.[3] The strain effect of the Ba_2ZnF_6 host lattice is comparatively much larger (ρ_s = 10.5 pm, Table III), resulting in an energy b of about 1000 cm^{-1} [with $\gamma = V(Ba_2CuF_6)$]. With the same calculation procedure as for the $K_2Zn_{1-x}Cu_xF_4$ compounds a radial distortion parameter $\rho_0 \simeq 32.5$ pm is deduced for $Ba_2Cu_{0.1}Zn_{0.9}F_6$ from the energetic position of the lowest wavenumber ligand field band ($4E_{JT}$ = 6300 cm^{-1}). Assuming that the ratio of the linear and the nonlinear coupling constants is the same as that in (D), which seems reasonable, we calculate $b/\beta \simeq 14$. This value characterizes the situation with only one minimum at 180° [(B), Figure 14, $b \geq 9\beta$]. Indeed the mixed crystals $Ba_2Zn_{1-x}Cu_xF_6$ show g values corresponding to eq 10 and a pure d_{z^2} ground state up to $x \simeq 0.3$. The **g** tensor is not markedly temperature dependent, which may be taken as an evidence for a deep and steep potential well, in agreement with the large b/β ratio. At about $x \approx 0.4$ ($4E_{JT}$ = 7000 cm^{-1}) a slight increase of $g_\parallel$ is found, again in close correspondence to the calculation, which yields $b/\beta \simeq 9$. After all the set of numerical values for the various Jahn–Teller energy parameters is consistent with the available experimental results. The Rb compounds seem to behave quite similar to the $K_2Zn_{1-x}Cu_xF_4$ mixed crystals.

Instead of choosing the model discussed above, we might have described the EPR results in terms of a pseudo Jahn–Teller effect $(A + B) \times \beta$. Because the Jahn–Teller energy is much larger than the splitting effects induced by the host lattice, however, a treatment based on the $E \times \epsilon$ coupling is certainly more justified.

The mixed crystals in the *concentration range* $0.1 \lesssim x \lesssim 0.4_5$ are not well defined. A decrease of the Cu^{2+} concentration from $x = 0.45$ to about $x \approx 0.3$ strongly broadens the EPR signals (Figure 13), which are still of the exchange-narrowed type, however—with g values not too far away from those in the $x \gtrsim 0.4_5$ region. The EPR analysis of a single crystal with 26 mol % Cu^{2+} reveals a strongly temperature-dependent **g** tensor similar to those with $x \lesssim 0.1$ and is probably already of the dynamic type (Table IV). Rather unexpected between $0.25 \gtrsim x \gtrsim 0.10$, both types of signals, those characteristic of "dynamic" behavior and exchange-type ones, overlap in the powder EPR spectra of the K- and Rb-mixed crystals (Figure 13). We think that Cu^{2+} clusters of different sizes within the two-dimensional layers of the host structure account for the observations. Calculations of Friebel[23] demonstrate how the probability of finding clusters of a certain size in two-dimensional nets depends upon the concentration of the substituting ion. They indicate that at $x \simeq 0.45$ half of the copper is part of clusters containing at least 12 ions already. For $x \simeq 0.25$ on the other hand, half of the Cu^{2+} ions are still isolated. While these results are in accord with the experimental data above $x = 0.45$ and below $x = 0.10$, the presence of exchange-narrowed EPR signals of larger intensity in the range $0.10 \lesssim x \lesssim 0.25$ is hardly understandable and may be caused by a nonstatistical Cu^{2+} distribution in the host structure as the consequence of the special preparation conditions. The interpretation of these spectra (Figure 13) as due to orthorhombic signals is ruled out, because the small splitting of $g_\perp$ would not agree with the large 2α values (Table V).

A molecular **g** tensor, which corresponds to *one* of the two minima symmetrical to $\varphi = 180°$, has never been observed, neither in the compounds under discussion nor for the $Ba_2Zn_{1-x}Cu_xF_6$ mixed crystals. An energy barrier of about 115 cm^{-1} between the minima and the saddlepoint at 180°, which may be considered as just high enough to localize the lowest radial vibronic state in either minimum, is expected for $b/\beta \simeq 2$. This ratio corresponds to $\rho_0 \simeq 40$ ppm and a Cu^{2+} concentration of $x \approx 0.8$ [(A)], which exceeds the critical x value (≈0.3) for the observation of exchange coupling in the EPR spectra by far.

Summary and Conclusion

The EPR spectra of mixed crystals $K(Rb)_2Zn_{1-x}Cu_xF_4$ have the symmetry of tetragonally compressed octahedra. A closer inspection shows, however, that the **g** tensor in the high-concentration range $x \geq 0.4_5$ is exchange narrowed, reflecting the antiferrodistortive order of essentially elongated CuF_6 octahedra, which is observed structurally.[11] The constituting sublattices have angular parameters φ smaller than 120° and larger than 240° (Figure 11a). At low Cu^{2+} concentrations $x \lesssim 0.10$ the EPR spectra are still determined by two minima symmetrically to 180°. The φ parameters of these minima are found to change from 156 to 150° and from 204 to ≃210°, respectively, with increasing x (Table V). The energy barrier is low enough to allow motional narrowing, leading to compressed CuF_6 octahedra in time average (Figure 11b). The ground state is not pure d_{z^2} but contains appreciable admixtures of $d_{x^2-y^2}$. The situation with only one minimum at 180° could not be verified, even at very low Cu^{2+} concentrations. It was found, however, in mixed crystals of $Ba_2Zn_{1-x}CuF_6$ ($x \lesssim 0.3$) as the consequence of the considerable strain imposed on Cu^{2+} by the comparatively larger tetragonal compression of the ZnF_6 octahedra in the Ba_2ZnF_6 host lattice.[3] A continuous transition from the "dynamic" EPR spectra with smaller deviations of φ from 180° to the exchange-narrowed signals at high x values could not be observed. Because of the presence of Cu^{2+} clusters, which presumably widely vary in size between $0.25 < x \lesssim 0.45$, the EPR spectra in this bridging concentration range were not well defined.

The reason for the appreciable changes of ρ_0 and φ_0 with increasing x [Figures 8 and 11, (A)] may be seen in the continuous replacement of Zn^{2+} by Cu^{2+} ions in the neighborhood of any CuF_6 entity. Cooperative elastic interactions between the CuO_6 polyhedra in the host structure become increasingly important and shift the linear (E_{JT}) and nonlinear coupling energies (β) to higher values. This means, that the strain influence of the host structure gradually looses its influence with increasing x, and hence the angular parameters move toward φ = 120 and 240°. Above $x \simeq 0.4_5$, at which concentration a transition from the K_2NiF_4 type to the K_2CuF_4 structure is likely to occur, a long range *cooperative Jahn–Teller order* with the symmetry of an antiferrodistortive pattern is observed. The corresponding molecular field tends to stabilize orthorhombic sublattices of $\pm Q_\epsilon$ symmetries[21]

(23) C. Friebel, *Acta Crystallogr., Sect. A*, **A36**, 259 (1980).

(Figure 1) and may equally be treated as a strain with δ_s = 90 and 270° (eq 12). Molecular fields of this symmetry seem still to be important at $x < 0.4_5$, however, if Cu^{2+} clusters above a certain critical size are considered only. Thus the observaton of two types of EPR signals in the intermediate concentration range indicates the presence of clusters above and below this critical size. This latter argument explains reasonably well the discontinuity in the shift of the φ parameters (Figure 11). The change in the elastic forces between the CuF_6 polyhedra due to the substitution of Zn^{2+} by Cu^{2+} ions is considerable in this specific host structure, which is related to the perovskite type. Similarly strong variations of the local distortions in dependence on the concentration of the Jahn-Teller cations have been observed in various other mixed-crystal series.[1,24]

The energy of the radial vibrations $\hbar\omega$ is calculated to be $\simeq$200 cm^{-1} for $x = 1$ and $\simeq$250 cm^{-1} for $x < 0.10$ (eq 5). These values seem reasonable in magnitude for metal-ligand vibrations in this type of compound. The angular energy, which induces the thermal fluctuation between the two sublattices can be estimated from eq 14[2] which holds for large values of $4E_{JT}\beta/(\hbar\omega)^2$. For K_2CuF_4 one obtains $\hbar\omega' \simeq 125$ cm^{-1}.

$$\hbar\omega' = 3\left(\frac{\beta}{2E_{JT}}\right)^{1/2}\hbar\omega \qquad (14)$$

It is finally interesting to compare the dynamic behavior in the low concentration range with the one described by Silver and Getz.[25] While in our system complete motional narrowing between minima of *equal* energies occurs, there is a small energy difference between them in Cu^{2+}-doped Tutton salts, which is obviously induced by an *orthorhombic* host lattice strain. The **g** tensor is orthorhombic but exhibits a tendency toward tetragonal symmetry with increasing temperature due to extensive thermal population of the higher of the two levels. The EPR spectra of the stochiometric complex $Cu(terpy)_2Br_2 \cdot 3H_2O$ exhibit a similar behavior with incomplete motional narrowing even at high temperatures.[22] After all $Ba_2Cu_xZn_{1-x}F_6$ mixed crystals with $x < 0.3$ are the only systems so far described, in which Cu^{2+} occupies a tetragonally compressed site with a pure d_{z^2} ground state.[1,3]

The assignment of the electronic transitions in the ligand field spectra, in particular at low Cu^{2+} concentrations, remains doubtful (Figure 8). The change of φ with increasing x is not reflected by any variation of the intensity distribution or additional splittings, as one would expect on the basis of the EPR results. The same observation was made for the $Ba_2Zn_{1-x}Cu_xF_6$ mixed crystals.

Acknowledgment. We gratefully acknowledge the measuring facilities at the Institut für Angewandte Kernphysik, Kernforschungszentrum Karlsruhe, and thank Dr. S. Klein for recording the neutron diffraction diagrams. D.R. appreciates the hospitality of Professor Hagenmuller and Dr. Tressaud during a sabbatical stay at the University of Bordeaux, in which this paper was written. We also would like to thank Drs. M. A. Hitchman and C. Friebel for valuable discussions.

Registry No. K_2ZnF_4, 37732-22-2; K_2CuF_4, 17712-46-8; Rb_2ZnF_4, 35944-46-8; Rb_2CuF_4, 17712-47-9.

(24) D. Reinen, H. O. Wellern, and C. Friebel, *Phys. Chem. Solids*, in press.

(25) B. L. Silver and D. Getz, *J. Chem. Phys.*, **61**, 638 (1974).

Contribution from the Christopher Ingold Laboratories, University College London, London WC1H OAJ, United Kingdom

Resonance Raman, Excitation Profile, and Electronic Structural Studies of Diruthenium Tetracarboxylate Complexes

ROBIN J. H. CLARK* and LINDSAY T. H. FERRIS

Received October 8, 1980

The resonance Raman spectra of the diruthenium carboxylate complexes $Ru_2(O_2CCH_3)_4Cl$, $[Ru_2(O_2CCH_3)_4(H_2O)_2]^+BF_4^-$, $Ru_2(O_2CH)_4Cl$, $Ru_2(O_2CC_2H_5)_4Cl$, and $Ru_2(O_2CC_3H_7)_4Cl$ have been recorded, at room temperature as well as at ca. 80 K, with exciting lines of wavenumber in the region of the electronic band which lies at ~21 000 cm^{-1} for each complex. The Raman band which is the most resonance enhanced in each case is that at 326-340 cm^{-1}. On the basis of studies of its depolarization ratio and of its lack of sensitivity to ^{18}O substitution in the case of the acetate complex, this band is assigned to the $\nu_1(a_{1g})$ fundamental, the Ru-Ru stretching mode (in D_{4h} nomenclature). A second band, at 369-432 cm^{-1}, has its intensity modified (although to a lesser extent) when the complexes are irradiated in the 21 000-cm^{-1} region. This band is also polarized, and on the basis of its shift (~5-13 cm^{-1}) on ^{18}O substitution of the acetate complex, the band is unambiguously assigned to the $\nu_2(a_{1g})$ fundamental, the symmetric Ru-O stretching mode. The excitation profiles of these two Raman bands of each complex are discussed. These results, together with polarization dispersion results, imply that the resonant electronic transition is electric-dipole allowed in axial (z) polarization, a result which is in agreement with a recent molecular orbital treatment in which the transition was given the assignment $6e_u \rightarrow 6e_g$, $O(\pi) \rightarrow \pi^*$. Excitation to the π^* state would lead to a decrease in Ru-Ru as well as in Ru-O π bonding and thus to a lengthening of both Ru-Ru and Ru-O bonds in the $6e_g$ excited state. On resonance with the $6e_u \rightarrow 6e_g$ transition, therefore, progressions in ν(RuRu) as well as ν(RuO) would be expected, as observed, for the acetate complex. The other complexes show unexplained differences in this respect since they display $\nu_2 + \upsilon_1\nu_1$ but not $\upsilon_2\nu_2$ progressions. The observation of these progressions enables both harmonic wavenumbers and anharmonicity constants to be calculated.

Introduction

The dimeric complexes of ruthenium formed with bridging carboxylate ligands, $Ru_2(O_2CR)_4Cl$, were reported in 1966 by Stephenson and Wilkinson[1] and were formulated as involving mixed +2,+3 oxidation states of ruthenium. The paramagnetism of the complexes is indicative of the presence of three unpaired electrons per dimer. The key structural features of the butyrate complex were established by Cotton et al.[2] to consist of four bridging butyrate groups per dimer,

(1) Stephenson, T.A.; Wilkinson, G. *J. Inorg. Nucl. Chem.* **1966**, *28*, 2285.

(2) Bennet, M. J.; Caulton, K. C.; Cotton, F. A. *Inorg. Chem.* **1969** *8*, 1.

0020-1669/81/1320-2759$01.25/0